W phase inversion and tsunami inundation modeling for tsunami early warning: case study for the 2011 Tohoku event

Aditya Riadi Gusman and Yuichiro Tanioka
Institute of Seismology and Volcanology, Hokkaido University, Japan

Abstract

Centroid moment tensor solutions for the 2011 Tohoku earthquake are determined by W phase inversions using 5 min and 10 min data recorded by the Full Range Seismograph Network of Japan (F-net). By a scaling relation of moment magnitude to rupture area and an assumption of rigidity of 4×10^{10} N m^{-2}, simple rectangular earthquake fault models are estimated from the solutions. Tsunami inundation area and heights are simulated in the Sendai Plain, Minamisanriku, and Rikuzentakata using the estimated fault models. Then the simulated tsunami inundation area and heights are compared with the observations. Even the simulated tsunami heights and inundations from the W phase solution that used only 5 min data are considerably similar to the observations. The results are improved when using 10 min of W phase data. These show that the W phase solutions are reliable to be used for tsunami inundation modeling. Furthermore, the technique that combines W phase inversion and tsunami inundation modeling can produce results that have sufficient accuracy for tsunami early warning purposes.

Keywords: Tsunami early warning; tsunami inundation modeling; W phase inversion.

1. Introduction

On 11 March 2011, only 3 minutes after the origin time of the 2011 Tohoku earthquake (14:46 JST), the Japan Meteorological Agency (JMA) warned that tsunami larger than 3 m would hit east coast of Tohoku area. The actual tsunami that struck the coastal area was more than 10 m and reached 40 m in some places (Mori et al., 2012). The JMA used strong motion data to get the Mjma = 7.9 that was then used to generate the first tsunami warning of the 2011 Tohoku earthquake. After an offshore tsunami data was analyzed by the JMA about 25 min latter, the tsunami warning was updated in which the estimated coastal tsunami heights was larger than 10 m. After 54 minutes from the earthquake's origin time, a magnitude Mw 8.8 was obtained for the earthquake (http://www.jma.go.jp/jma/en/2011_Earthquake/Information_on_2011_Earthquake.html).

The JMA issued three types of messages for coastal areas in Japan during the 2011 event, which are tsunami advisory, tsunami warning, and major tsunami warning. These advisory and warning messages are visualized as color-coded lines along the Japanese coastlines and broadcast on television (Figure 1). These messages save many lives but apparently were not enough for many other people to immediately evacuate. Large-scale maps of the predicted tsunami inundation area and heights might have been able to better illustrate the dangers that threaten and convinced them to evacuate immediately.

To produce the map of predicted tsunami inundation, accurate moment magnitude estimation is required. The W phase, a distinct long-period (200 to 1000 sec) phase that arrives before S phase, can be used for rapid and robust determination of great earthquake source parameters with sufficient accuracy (Kanamori and Rivera, 2008). The Full Range Seismograph Network of Japan (F-net) provides enough data to determine the 2011 Tohoku earthquake's magnitude. Moment tensor solution for the earthquake can be estimated by using a W phase inversion algorithm developed by previous studies (Kanamori and Rivera, 2008; Duputel et al., 2011).

In this study, the 2011 earthquake parameters such as the centroid location, magnitude and focal mechanism are estimated using the W phase data. A magnitude to area scaling relationship is then used to estimate simple rectangular fault models for tsunami inundation simulation. The Sendai Plain in Miyagi prefecture, Minamisanriku in Miyagi prefecture, and Rikuzentakata in Iwate prefecture (Figure 2) are selected for tsunami inundation simulation. To evaluate the computed tsunami inundation areas for a tsunami early warning, we compare the simulated tsunami inundation areas and tsunami heights with the observations. Finally, we discuss the possibility of using the W phase inversion and tsunami inundation modeling for tsunami early warning purpose.

2. Data

2.1. Seismic wave data for W phase inversion

We retrieved the LH and LL channels from global networks through the Incorporated Research Institutes for Seismology (IRIS) data center and from F-net through the National Research Institute for Earth Science and Disaster Prevention data center. These data are used to estimate moment tensor of the 2011 Tohoku earthquake by W phase inversion.

2.2. Bathymetry data for tsunami numerical simulation

The bathymetry dataset used for tsunami simulation is based upon the General Bathymetric Chart of the Oceans (GEBCO) 30 arc-sec grid resolution, Japan Hydrographic Association's M7005 bathymetric contour data, Advanced Spaceborne Thermal Emission and Reflection Radiometer (ASTER) Global Digital Elevation Model (GDEM), and Geospatial Information Authority of Japan (GSI) topographic contour maps. Publicly available ASTER GDEM topographic data with grid resolution of 30 m is not very accurate, coastal terrain and infrastructure such as ports are poorly modeled in the GDEM. Therefore, for topography data below 50 m elevation, we manually digitized topographic contours from the GSI maps and to improve the coastline and used the ASTER GDEM data as the background topographic data.

2.3. Tsunami inundation data of the 2011 Tohoku tsunami

The great 2011 earthquake generated a large tsunami that devastated coastal areas along the east coast of Tohoku. Post-tsunami fieldwork along the coast of Japan provided more than 5,200 measurements of inundation, including tsunami height and run-up (Mori et al., 2012). In general, maximum tsunami run-up heights greater than 10 m are distributed along 500 km of coast (Mori et al., 2012). Tsunami height exceeds 20 m at heads of V-shaped bays and apexes of peninsulas, and exceptional tsunami run-up heights of over 35 m was measured at a small valley, Aneyoshi, on Omoe peninsula (Shimozono et al., 2012). The inundation limit of the tsunami was also mapped in every major town in the Sanriku coast and Sendai area.

The Sendai Plain is a vast flat area, which is dominated by rice fields near the coastline. The flat area has topography of lower than 5 m from the coastline until up to 5 km inland which was inundated during the 2011 Tohoku tsunami (Figure 3). The maximum tsunami inundation height was 19.5 m, and the mean tsunami inundation height near the shoreline was about 10 m (Mori et al., 2012). In Minamisanriku, the maximum tsunami run-up was 27 m. The tsunami inundation heights and run-ups were mostly range from 14 to 16 m. The inundation continued as far as 3 km inland (Figure 4), following river valleys into the mountainous terrain (MacInnes et al., 2012). In Rikuzentakata, the maximum tsunami run-up height was 21.6 m. The tsunami inundation heights and run-ups were mostly range from 14 to 16 m. Similar to what was observed in Minamisanriku, the inundation in Rikuzentakata continued following river valleys in the mountainous terrain, but in here, the tsunami reached as far as 5 km inland (Figure 5).

3. Method

3.1. W phase inversion

We used the W phase inversion algorithm (Kanamori and Rivera, 2008; Duputel et al., 2011) to estimate moment tensor of the 2011 Tohoku earthquake. The W phase source inversion algorithm was specifically developed to estimate the magnitude, centroid location and mechanism of great earthquakes like the 2011 Tohoku earthquake (Kanamori and Rivera, 2008; Duputel et al., 2011). Time domain deconvolution is used to retrieve ground displacement and then it is filtered between 1 and 5 mHz using 4^{th} order of the Butterworth filter. The time window is from the P wave until 15 times the distance between point source to the station. For more details of the W phase inversion method see Kanamori and Rivera (2008), Duputel et al. (2011), and Duputel et al., (2012).

We estimate the moment tensor solutions for the 2011 Tohoku earthquake by the W phase inversion algorithm using 5 min and 10 min data of LH and LL channels belonging to the F-net. We also estimate a final moment tensor solution using data retrieved from global seismic networks through the Incorporated Research Institutes for Seismology (IRIS) data center.

3.2. Scaling relations

Scaling relations are needed to estimate rupture area from earthquake's moment magnitude. The moment magnitude (Mw) to fault area (A) relation of Wells and Coppersmith (1994) are widely used in seismic hazard analysis. The relationship was derived from a data base including all slip types of continental interplate or intraplate earthquakes, with the exception of subduction zones earthquakes both those at the interface and those within the oceanic slab. There are other recent scaling relationships that focused on continental events (Hanks and Bakun, 2002) and that focused on subduction zone events (Blaser et al., 2010).

The major slip area of the 2011 Tohoku earthquake is approximately 150 km wide by 300 km long, which is relatively compact compared with the aftershock region (Ammon et al., 2011; Pollitz et al., 2011; Gusman et al., 2012). For this particular event, the major slip area estimated by the previous studies is similar to rupture area estimated by the relationship of Hanks and Bakun (2002). Therefore, in this study, the magnitude to area scaling relationship ($Mw = 4/3 \log A + 3.03$) for rupture area larger than 1000 km^2 of Hanks and Bakun (2002) is used. The fault length (L) and fault width (W) are calculated from the estimated rupture area by a simple relationship of fault length (L) = 2 × fault width (W). Then a slip amount can be estimated from the ruptured area and scalar moment by assuming the rigidity of along the plate interface, in this study we assume that the rigidity is 4×10^{10} N m^{-2}.

3.3. Tsunami Inundation Model

To simulate tsunami inundation, the non-linear shallow water equations in a Cartesian coordinate system are solved by the finite different scheme (Goto et al., 1997). Tsunami inundation is numerically computed using moving boundary condition. Discharge across the boundary between two cells is calculated if the ground height in the dry cell is lower than the water level in the submerged cell; otherwise, discharge is considered to be zero (Imamura, 1996). In this study, tsunami inundation in the Sendai Plain, Minamisanriku, and Rikuzentakata are simulated. To simulate tsunami inundation in the Sendai Plain, a grid system with grid size of 50 m is used. While for Minamisanriku and Rikuzentakata, the grid system that is used has a grid size of 15 m. For all sites, the Manning's roughness coefficient is assumed to be 0.025.

3.4. Comparisons of tsunami simulations and observations

We used the measured tsunami data for comparison with simulated tsunami to evaluate the performance of each source model in reproducing the actual tsunami height and inundation. For each post-tsunami observation at a simulated site, the height above sea level of the simulated tsunami (H_{sim}) is compared with the actual measurement (H) at the same position, or the closest numerically inundated point when the observed point did not numerically inundated. The ratios between simulated and observed tsunami heights (H_{sim}/H) at each site are plotted in a histogram with interval of 10%. The kurtosis (β) of the ratio distribution shows how well the simulation produced the overall observed pattern of inundation. The more peaked and narrow the histogram, or larger the kurtosis value, the better the simulation was able to reproduce the pattern of observation.

4. Results and discussion

We estimated three centroid moment tensor solutions, two of which are using 5 min data and 10 min of W phase data recorded at Japan stations, and a final W phase centroid moment tensor (WCMT) solution (Figure 2) using data recorded in global networks. The final moment tensor solution providing Mw estimation of 9.0, strike = 200°, dip = 13°, rake = 89° (Table 1), and centroid location is up-dip the epicenter (Figure 2), which are consistent with the moment tensor solutions provided by Duputel et al. (2011) and the USGS W phase solution. The W phase solution using 5 min data after the p wave arrives at the Japanese stations providing Mw estimation of 9.0, which is consistent with the final W phase moment tensor solution. However, the centroid location and focal mechanism are poorly resolved. While the solution using 10 min of W phase data providing Mw estimation of 9.1 that is slightly larger than Mw 9.0 from the final moment tensor solution. The earthquake parameters of strike, dip, and rake angles obtained using 10 min of W phase data are similar to those of the final moment tensor solution. The centroid locations of the solutions estimated using the Japanese F-net data are poorly resolved because of the limited azimuthal coverage. For simplicity, we will refer the centroid moment tensor solutions estimated using 5 min, 10 min, and the global data as Solution 1, Solution 2, and Solution 3, respectively.

Rupture areas calculated for given moment magnitudes of Mw 9.0 and Mw 9.1 by Mw = 4/3 log A + 3.03 (Hanks and Bakun, 2002) are approximately 30,000 and 36,000 km^2, respectively. By applying a relationship of fault length (L) = 2 × fault width (W), we obtained fault dimension of L = 123 km and W = 246 km for Mw 9.0, and L=134 km and W = 268 km for Mw 9.1. By assuming the rigidity of 4×10^{10} N m^{-2}, the slip amount calculated from the scalar moments of the Solutions 1, 2 and 3 are 31 m, 37 m, and 32 m, respectively (Table 1).

The simulated tsunami inundation areas from all source models and the observed tsunami inundation data for the Sendai Plain, Minamisanriku, and

Rikuzentakata are shown in Figure 3, 4, and 5, respectively. Histogram plot of ratio between simulated and observed tsunami height for each case are shown in Figure 6.

The simulated tsunami inundation area in the Sendai Plain from the simple source model of Solution 1 are underestimated the observation. While results of tsunami simulations from Solutions 2 and 3 resemble the actual tsunami inundation area and heights with mean ratios of 156% and 133%, respectively. Although the mean ratio from Solution 1 is the smallest compare to that from other solutions, the ratio distribution is rather random with local maxima and has the smallest kurtosis. The mean ratios and histogram plots for the Sendai Plain in Figure 6 show that the pattern of the simulated tsunami heights from Solution 3 resembles better the observations.

For Minamisanriku, tsunami simulation from Solution 1 is slightly underestimated the actual tsunami heights with mean H_{sim}/H ratio of 72% but has inundation area that is similar to the observation. While tsunami simulations from Solutions 2 and 3 give good results with mean H_{sim}/H ratios of 109% and 100%, respectively. High kurtoses of the ratio distributions from all simulations show that the simulated tsunami heights are consistent to the measured tsunami heights. The simulated tsunami inundations from all source models match well the observed inundation area.

For Rikuzentakata, tsunami simulations from Solutions 1 and 3 give good results of tsunami inundation area with mean H_{sim}/H ratios of 109% and 99%, respectively. High kurtoses of the ratio distributions from these simulations show that the simulated tsunami heights are consistent to the measured tsunami heights. Although tsunami simulation from Solution 2 produced slightly higher tsunami heights compare the measured ones with mean ratio of 140%, the simulated inundation area is also similar to the actual one. At this site, the difference in sizes of moment magnitude affected the simulated tsunami heights more than the difference in focal mechanisms.

Tsunami simulation results in the three locations from the three W phase solutions are considerably similar to the observed tsunami heights and inundations. Even though the W phase solution that used 5 min data has centroid location and focal mechanism with low accuracy, the resulting simulated tsunami heights and inundations are considerably similar to the observations. The simulated tsunami inundation area may give estimation of scale or threat of the incoming tsunami, and it could suggest for an immediate evacuation. The simulated tsunami inundation results are much improved when using the source model of the 10 min W phase solution. These suggest that the technique that combines the W phase inversion and tsunami inundation modeling can produce results that have sufficient accuracy for tsunami early warning purposes. A system that incorporates W phase inversion, pre-calculated tsunami propagation and tsunami inundation modeling might be able to estimate robustly the tsunami inundation area due to great earthquakes.

Because the scaling relationship of Hanks and Bakun (2002) was made to estimate the fault area of continental earthquakes, our selection to this scaling relationship over the one for subduction zone earthquakes by Blaser et al. (2010) in this study is counter intuitive. The estimated fault size for the Mw 9.1 earthquake

(Solution 2) by Blaser et al. (2010) relationships is 656 km x 212 km, which is larger than 268 km x 134 km estimated from Hanks and Bakun (2002) relationship. Hence the estimated slip amount on the larger fault size for the Mw 9.1 earthquake is 10 m, which is much smaller than 37 m for the smaller fault size. We also simulate the tsunami inundation in the Sendai Plain, Minamisanriku, and Rikuzentakata using the fault model with smaller slip amount. As expected, the simulated tsunami inundations in those locations are underestimating the observations. Figure 7 compares the maximum tsunami heights from both simple fault models, along the coastline of northeast Honshu on a 60 arc-seconds grid system. The comparison shows that the simulated tsunami heights from the fault model with the larger slip amount are larger between 37° to 40° N but similar else where. However, the simulated tsunami from the larger size fault model arrives noticeably sooner at locations to the north and south of the smaller size fault plane. In a case of real tsunami event, the worse scenario of tsunami inundation area, heights, and arrival time should be send to the coastal community for consideration of an immediate evacuation.

The time required for a high-resolution tsunami inundation model to finish is mainly depend on the computer speed, simulation domain and grid size. For this study we used a computer with an Intel® Core™ 2 Duo processor, running at 3.00 GHz, which supported by 4 GB of memory. To simulate 100 min of tsunami propagation and inundation in Sendai, Minamisanriku, Rikuzentakata, and Taro, the time required are 16.9 min, 34.7 min, 14.6 min, and 43.7 min, respectively.

Conclusions

We estimated three centroid moment tensor solutions where two of which are estimated using 5 min data, 10 min of W phase data recorded at the Japan F-net stations, and another one is a final W phase centroid moment tensor solution for the 2011 Tohoku earthquake using the global data. A scaling relation (Mw = 4/3 log A + 3.03) by Hanks and Bakun (2002) is used to calculate the rupture area from the moment magnitude. Then by assuming rigidity of 4×10^{10} N m^{-2} along the plate interface and a relationship between the length and width of the rupture area ($L = 2 \times W$), we obtained earthquake source parameters for tsunami inundation modeling.

Tsunami inundation area and heights are simulated in the Sendai Plain, Minamisanriku, and Rikuzentakata using the three estimated fault models for the 2011 Tohoku earthquake. Even the simulated tsunami heights and inundations from the W phase solution that used only 5 min data are considerably similar to the observations. The results are improved when using 10 min of W phase data. These show that the W phase solutions are reliable to be used for tsunami inundation modeling. Furthermore, the technique that combines the W phase inversion and tsunami inundation modeling can produce results that have sufficient accuracy for tsunami early warning purposes.

References

Ammon, C. J., Lay T., Kanamori, H., and Cleveland, M. (2011), A rupture model of the 2011 off the Pacific coast of Tohoku earthquake. Earth Planets Space, 63, 693-696, doi: 10.5047/eps.2011.05.015

Blaser, L., Krüger, F., Ohrnberger, M., and Scherbaum, F. (2010), Scaling relations of earthquake source parameter estimates with special focus on subduction environment. Bull. Seism. Soc. Am., 100 (6), 2914-2926, doi: 10.1785/0120100111

Duputel, Z., Rivera, L., Kanamori, H., and Hayes, G. (2011), Real-time W phase inversion during the 2011 off the Pacific coast of Tohoku earthquake. Earth Planets Space, 63, 535-539, doi: 10.5047/eps.2011.05.032

Duputel, Z., Rivera, L., Kanamori, H., and Hayes, G. (2012), W phase source inversion for moderate to large earthquakes (1990-2010). Geophys. J. Int., 189 (2), 1125-1147, doi: 10.1111/j.1365-246X.2012.05419.x

Goto, C., Ogawa, Y., Shuto, N., and Imamura, F. (1997), Numerical method of tsunami simulation with the leap-frog scheme, IUGG/IOC TIME project, IOC manual and guides, UNESCO, 35, pp. 1-126, 1997.

Gusman, A. R., Tanioka, Y., Sakai, S., and Tsushima, H. (2012), Source model of the great 2011 Tohoku earthquake estimated from tsunami waveforms and crustal deformation data, Earth Planet. Sci. Lett., 341-344, 234-242, doi: 10.1016/j.epsl.2012.06.006

Hanks, T. C., and Bakun, W. H. (2002), A bilinear source-scaling model for M-log A observations of continental earthquakes. Bull. Seism. Soc. Am., 92 (5), 1841-1846.

Imamura, F. (1996), Review of tsunami simulation with a finite difference method, in *Long-Wave Runup Models*, edited by H. Yeh, P. Liu, and C. Synolakis, 403 pp., World Scientific, Singapore.

Kanamori, H., and Rivera, L. (2008), Source inversion of W phase: speeding up seismic tsunami warning. Geophys. J. Int., 175, 222-238, doi: 10.1111/j.1365-246X.2008.03887.x

MacInnes, B. T., Gusman, A. R., LeVeque, R. J., Tanioka, Y. (2012), Comparison of earthquake source models for the 2011 Tohoku event using tsunami simulations and near field observations. Bull. Seism. Soc. Am., (In press).

Mori, N., Takahashi, T. and The 2011 Tohoku Earthquake Tsunami Joint Survey Group (2012), Nationwide post event survey and analysis of the 2011 Tohoku earthquake tsunami. Coastal Eng. J., 54(1), 1250001, doi: 10.1142/S0578563412500015

Pollitz, F. F., Bürgmann, R., and Banerjee, P. (2011), Geodetic slip model of the 2011 M9.0 Tohoku earthquake. Geophys. Res. Lett., 38, L00G08, doi:10.1029/2011GL048632

Shimozono, T., Sato, S., Okayasu, A., Tajima, Y., Fritz, H.M., Liu, H., and Takagawa, T. (2012), Propagation and Inundation Characteristics of the 2011 Tohoku Tsunami on the Central Sanriku Coast. Coastal Eng. J., 54(1), 1250004, doi:10.1142/S0578563412500040

Wells, D. L., and Coppersmith, K. J. (1994), New empirical relationships among magnitude, rupture length, rupture width, rupture area, and surface displacement. Bull. Seism. Soc. Am., 84 (4), 974-1002.

Table title

Table 1. Earthquake parameters of the W phase solutions for the 2011 Tohoku earthquake.

Figure captions

Figure 1. Tsunami warnings and advisory along the coastline of Japan during the 2011 Tohoku earthquake event that was broadcasted on television.

Figure 2. The W phase centroid moment tensor (WCMT) solutions and the fault planes for the 2011 Tohoku earthquake. Black star represents the epicenter of the 2011 Tohoku earthquake (JMA), white stars represent the centroid locations for the 5 min, 10 min, and final W phase centroid moment tensor solutions, and rectangles are fault planes for the solutions. Rectangles on the coast represent the tsunami inundation simulation sites.

Figure 3. Comparison between observed and simulated tsunami heights and inundation area in the Sendai Plain. (a) Blue bars and red points represent the observed and simulated tsunami height at blue points in Figure 3.b., respectively. The simulated tsunami inundation areas from the (b) final W phase solution, (c) 5 min W phase solution, and (d) 10 min W phase solution, black lines represent the observed limit of tsunami inundation.

Figure 4. Comparison between observed and simulated tsunami heights and inundation area in Minamisanriku. (a) Blue bars and red points represent the observed and simulated tsunami height at blue points in Figure 4.b., respectively. The simulated

tsunami inundation areas from the (b) final W phase solution, (c) 5 min W phase solution, and (d) 10 min W phase solution, black lines represent the observed limit of tsunami inundation.

Figure 5. Comparison between observed and simulated tsunami heights and inundation area in Rikuzentakata. (a) Blue bars and red points represent the observed and simulated tsunami height at blue points in Figure 5.b., respectively. The simulated tsunami inundation areas from the (b) final W phase solution, (c) 5 min W phase solution, and (d) 10 min W phase solution, black lines represent the observed limit of tsunami inundation.

Figure 6. Distribution of ratios between simulated and observed tsunami heights (H_{sim}/H).

Figure 7. Maximum tsunami heights along the coast from the fault models for Solution 2, blue line represents that from the larger fault size with 10 m slip amount and red line represents that from the smaller fault size with 37 m slip amount.

HD

NHK WORLD

NEWSLINE

itude of the quake is estimated at 7.9. BREAKING NEWS: A powerful quake hit the Paci

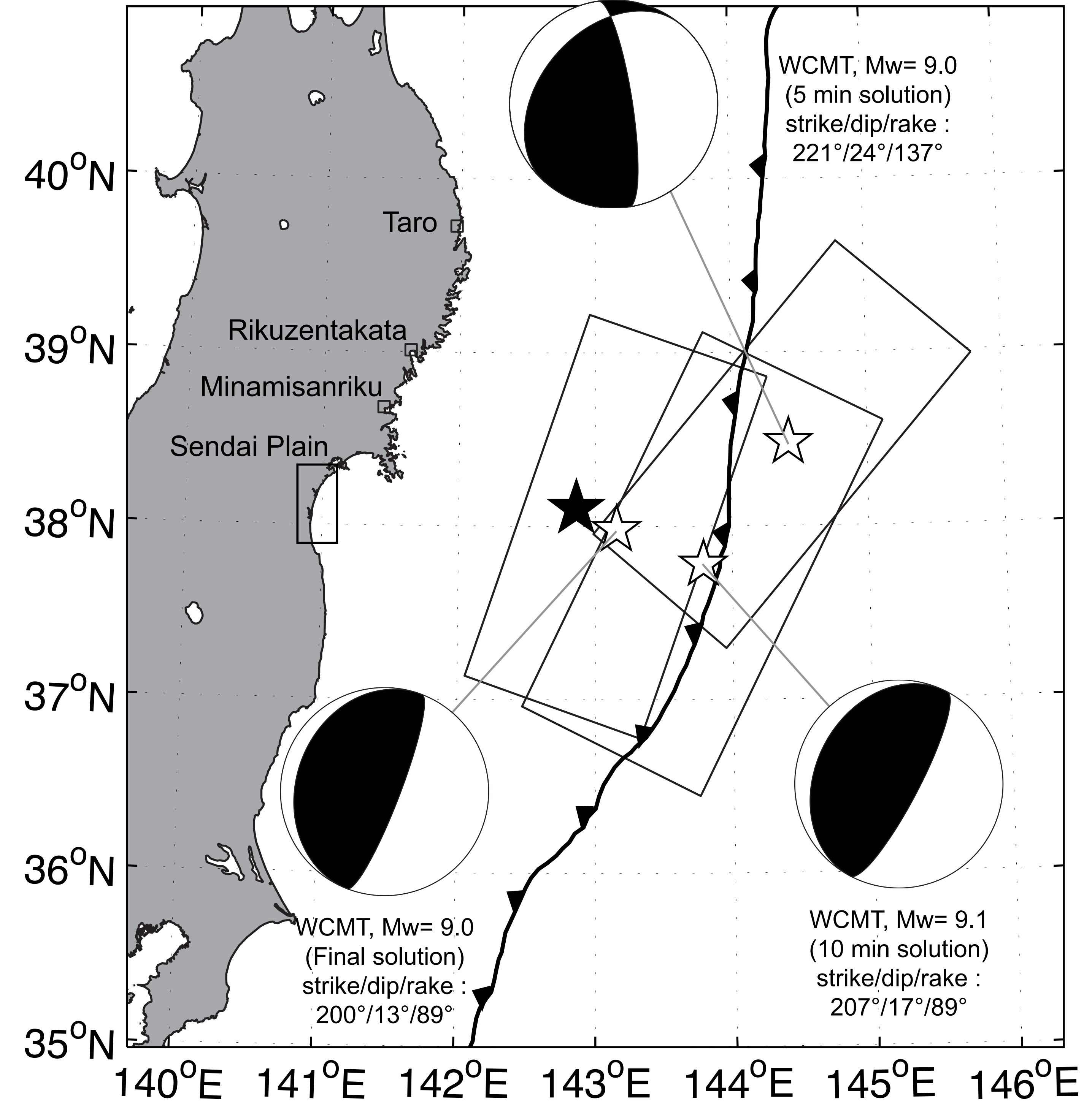

WCMT, Mw= 9.0
(5 min solution)
strike/dip/rake :
221°/24°/137°
Taro
Rikuzentakata
Minamisanriku
Sendai Plain
WCMT, Mw= 9.0
(Final solution)
strike/dip/rake :
200°/13°/89°
WCMT, Mw= 9.1
(10 min solution)
strike/dip/rake :
207°/17°/89°
40°N
39°N
38°N
37°N
36°N
35°N
140°E
141°E
142°E
143°E
144°E
145°E
146°E

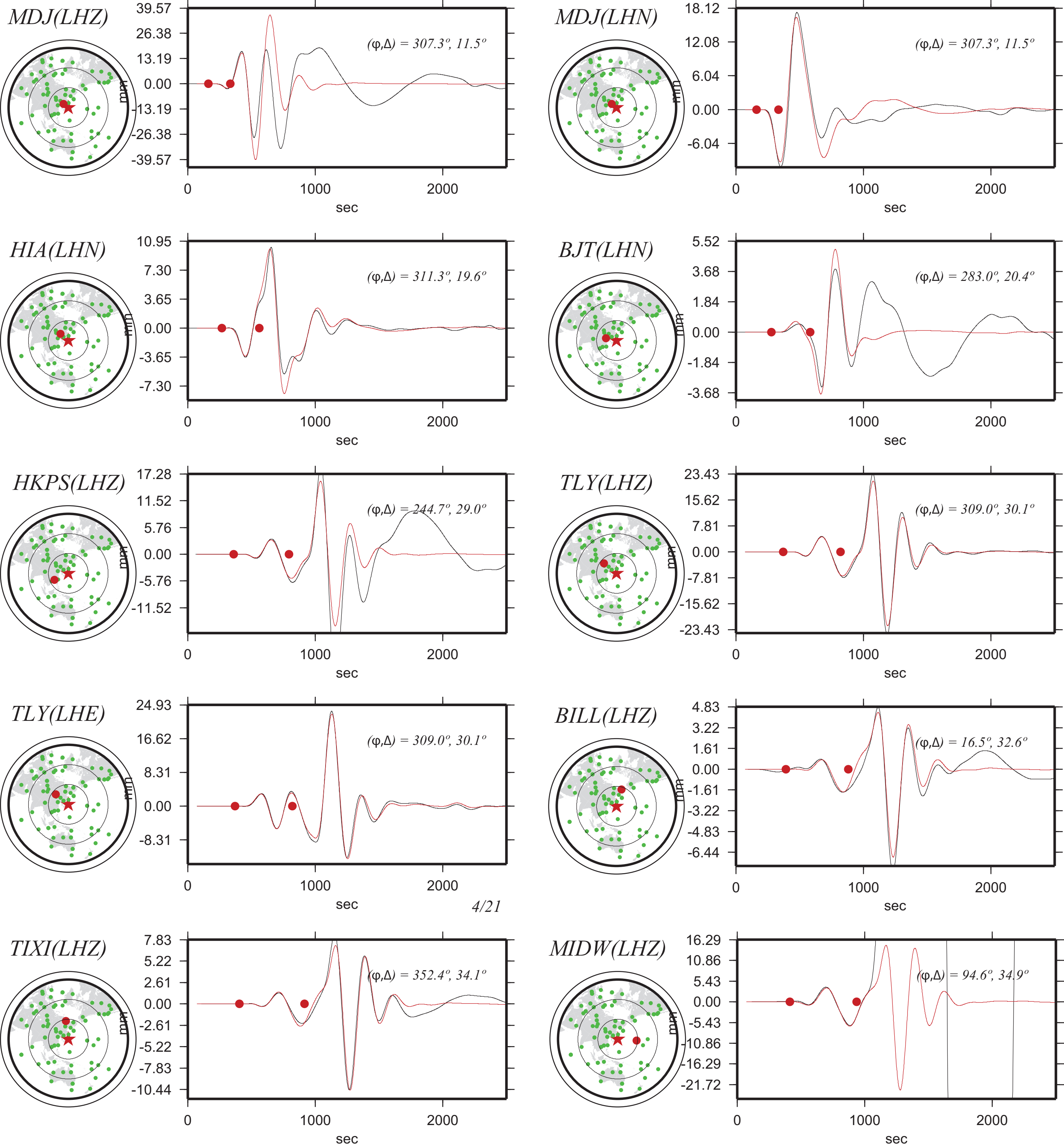

MDJ(LHZ)
(φ,Δ) = 307.3°, 11.5°
MDJ(LHN)
(φ,Δ) = 307.3°, 11.5°
HIA(LHN)
(φ,Δ) = 311.3°, 19.6°
BJT(LHN)
(φ,Δ) = 283.0°, 20.4°
HKPS(LHZ)
(φ,Δ) = 244.7°, 29.0°
TLY(LHZ)
(φ,Δ) = 309.0°, 30.1°
TLY(LHE)
(φ,Δ) = 309.0°, 30.1°
BILL(LHZ)
(φ,Δ) = 16.5°, 32.6°
TIXI(LHZ)
(φ,Δ) = 352.4°, 34.1°
MIDW(LHZ)
(φ,Δ) = 94.6°, 34.9°
mm
sec
0
1000
2000
4/21

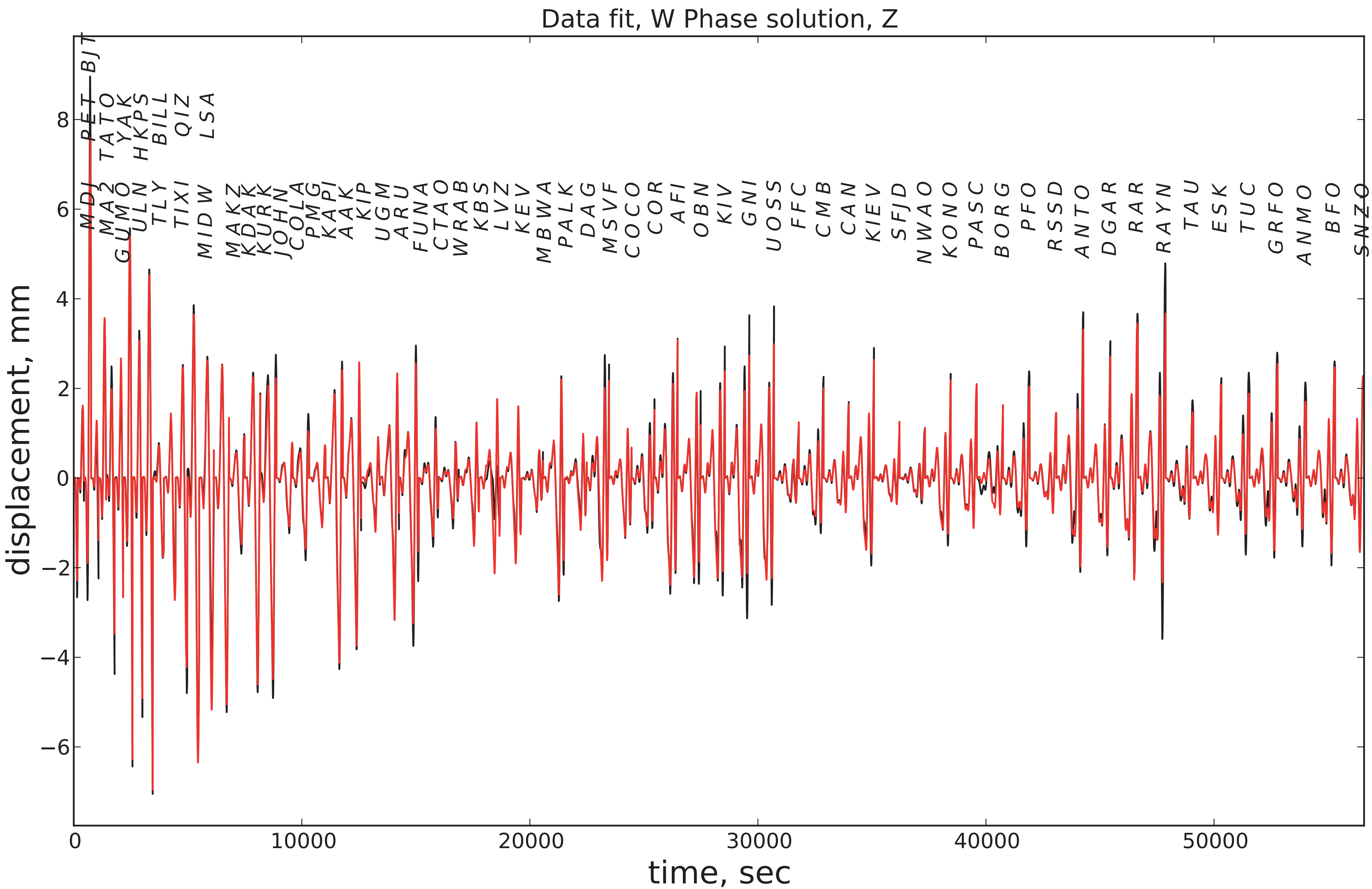

Data fit, W Phase solution, Z
displacement, mm
time, sec
−6
−4
−2
0
2
4
6
8
0
10000
20000
30000
40000
50000
BJT
PET
TATO
YAK
HKPS
BILL
QIZ
LSA
MDJ
MA2
GUMO
ULN
TLY
TIXI
MIDW
MAKZ
KDAK
KURK
JOHN
COLA
PMG
KAPI
AAK
KIP
UGM
ARU
FUNA
CTAO
WRAB
KBS
LVZ
KEV
MBWA
PALK
DAG
MSVF
COCO
COR
AFI
OBN
KIV
GNI
UOSS
FFC
CMB
CAN
KIEV
SFJD
NWAO
KONO
PASC
BORG
PFO
RSSD
ANTO
DGAR
RAR
RAYN
TAU
ESK
TUC
GRFO
ANMO
BFO
SNZO

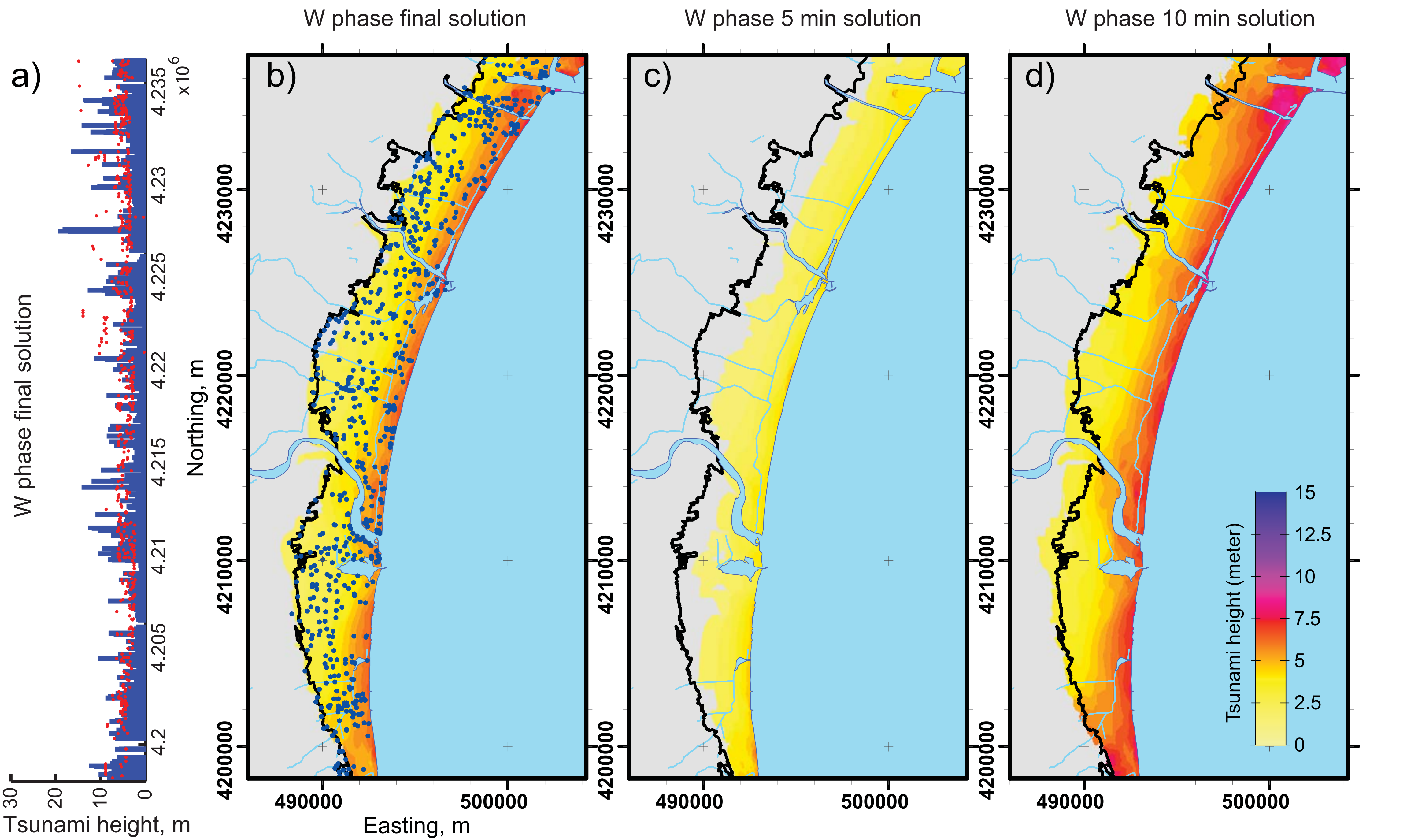

a)
W phase final solution
Tsunami height, m
30 20 10 0
x 10^6
4.235 4.23 4.225 4.22 4.215 4.21 4.205 4.2
W phase final solution
W phase 5 min solution
W phase 10 min solution
b)
c)
d)
Northing, m
Easting, m
4230000 4220000 4210000 4200000
490000 500000
Tsunami height (meter)
15 12.5 10 7.5 5 2.5 0

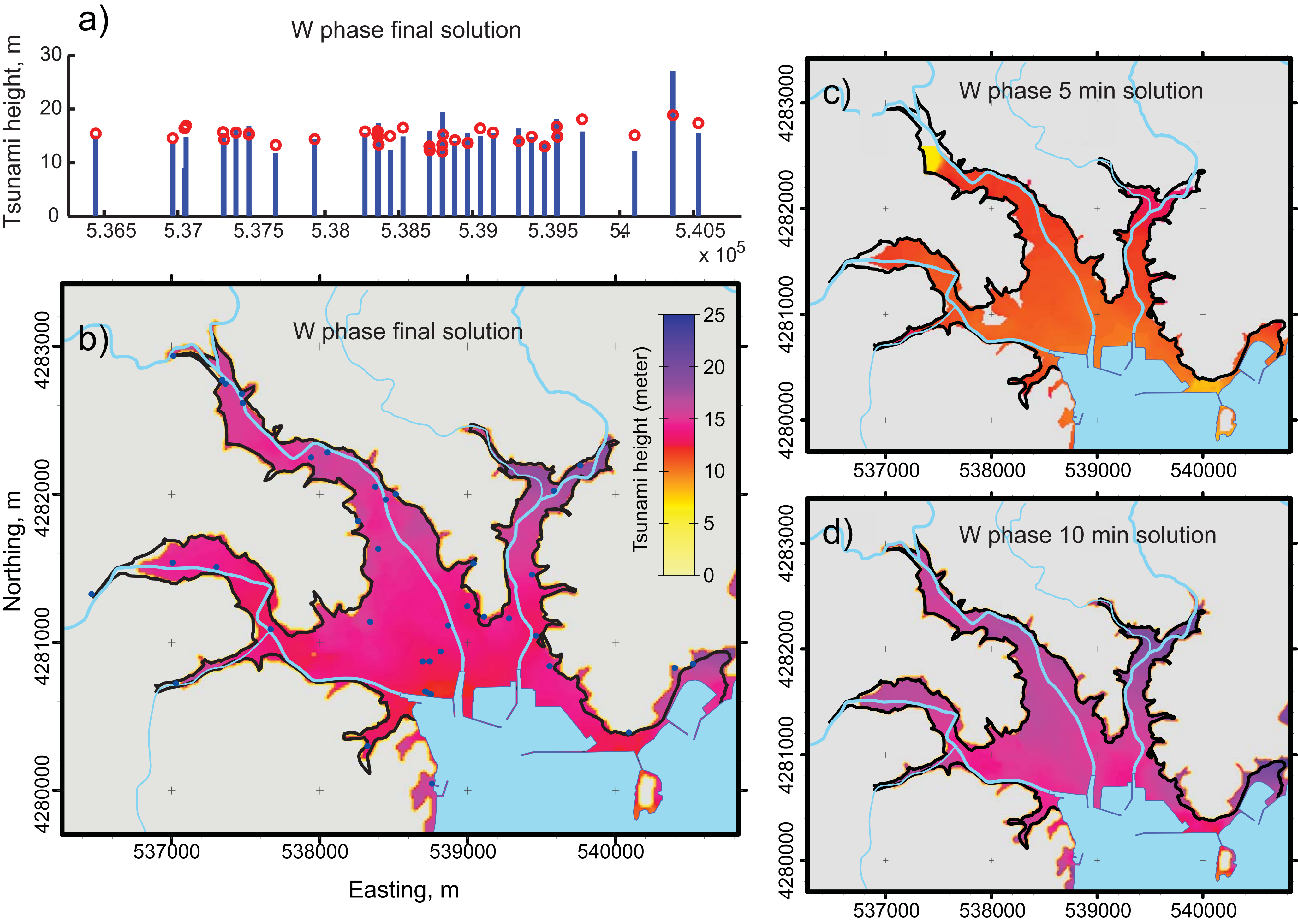
a)
W phase final solution
Tsunami height, m
30
20
10
0
5.365
5.37
5.375
5.38
5.385
5.39
5.395
54
5.405
x 10^5
b)
W phase final solution
Tsunami height (meter)
25
20
15
10
5
0
Northing, m
4283000
4282000
4281000
4280000
537000
538000
539000
540000
Easting, m
c)
W phase 5 min solution
d)
W phase 10 min solution

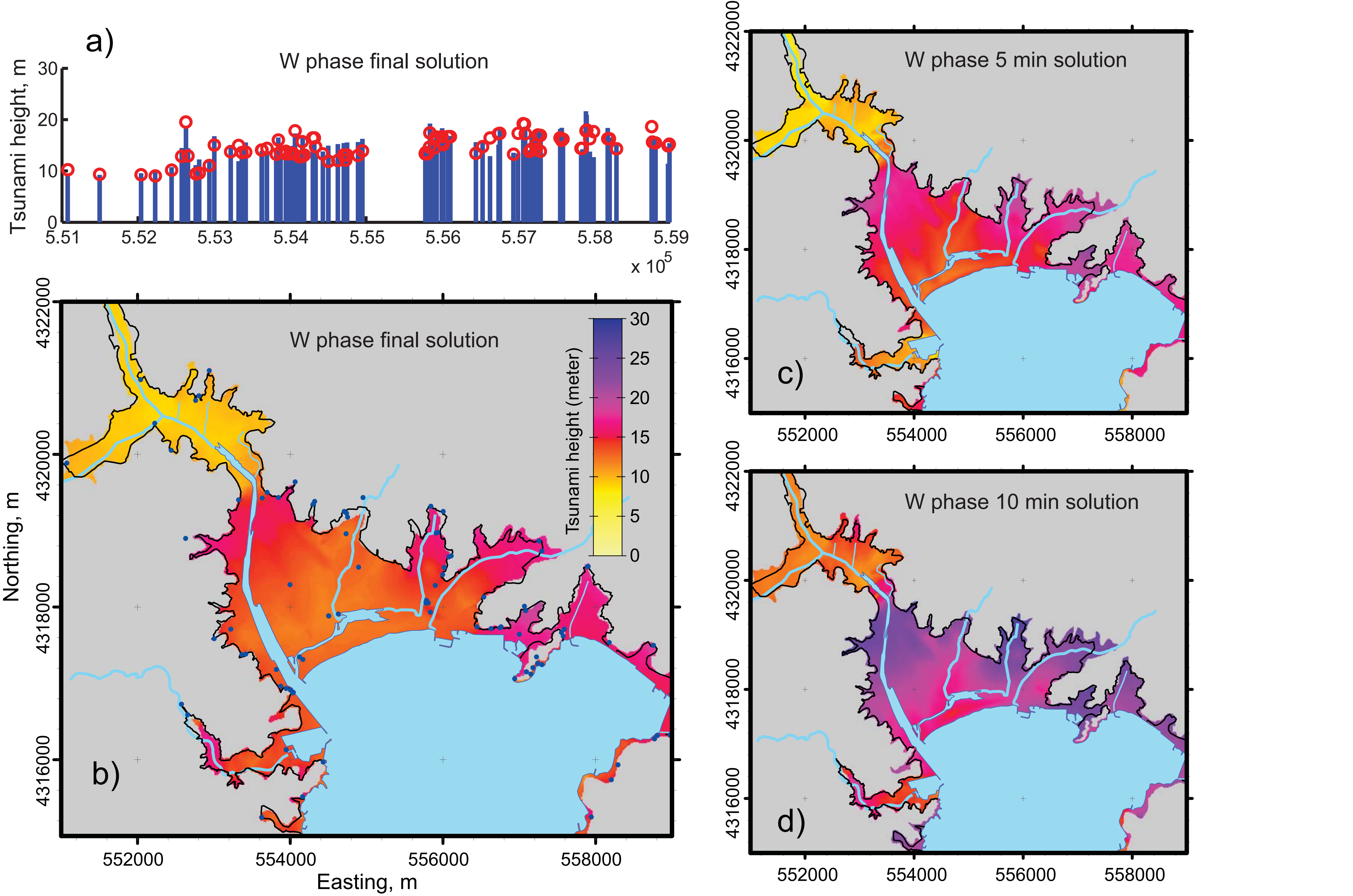

a)
W phase final solution
Tsunami height, m
30
20
10
0
5.51
5.52
5.53
5.54
5.55
5.56
5.57
5.58
5.59
x 10^5
b)
W phase final solution
Tsunami height (meter)
30
25
20
15
10
5
0
Northing, m
4322000
4320000
4318000
4316000
552000
554000
556000
558000
Easting, m
c)
W phase 5 min solution
d)
W phase 10 min solution

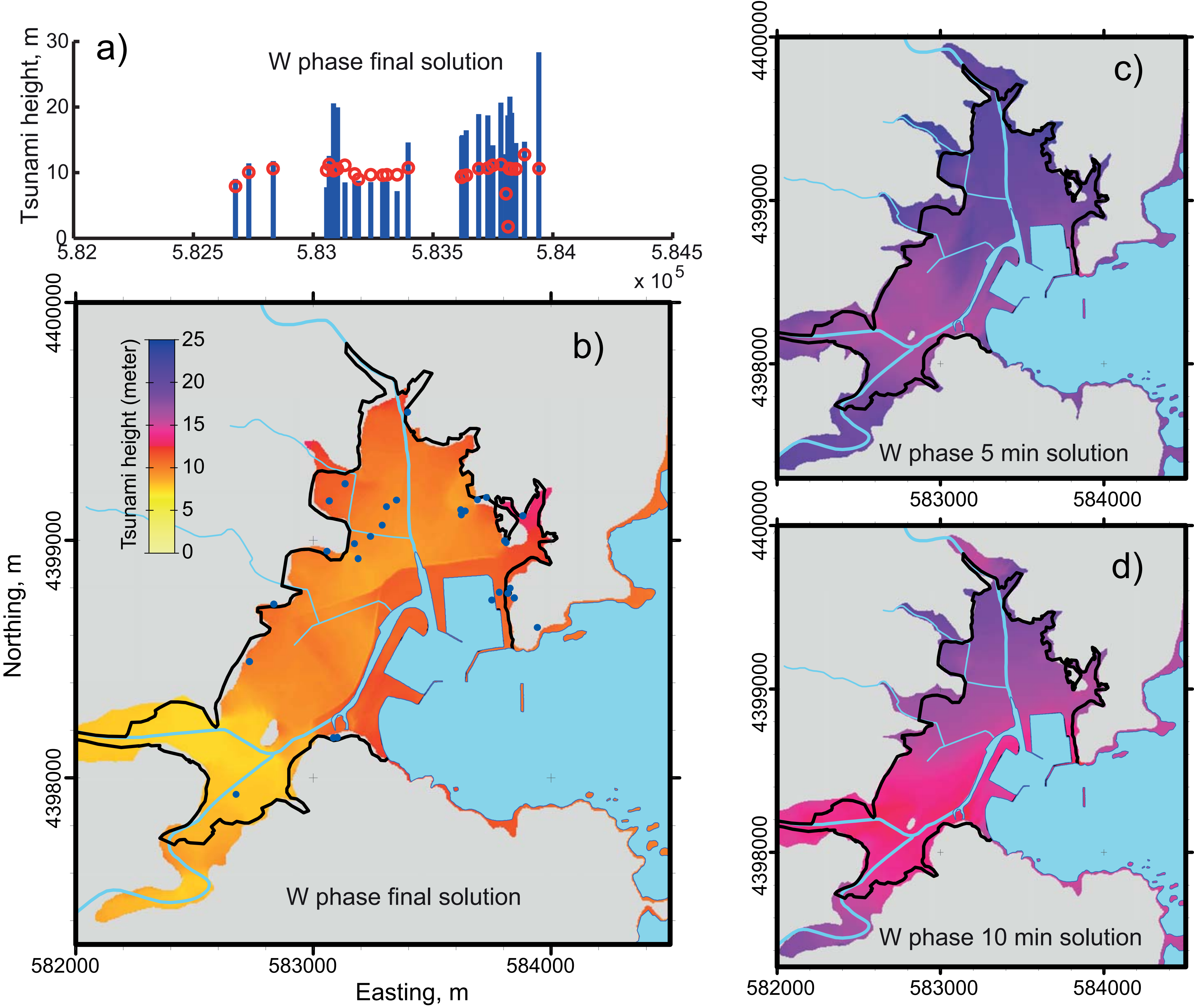

a)
W phase final solution
Tsunami height, m
30
20
10
0
5.82
5.825
5.83
5.835
5.84
5.845
x 10^5
b)
Tsunami height (meter)
25
20
15
10
5
0
W phase final solution
Northing, m
4400000
4399000
4398000
582000
583000
584000
Easting, m
c)
W phase 5 min solution
d)
W phase 10 min solution

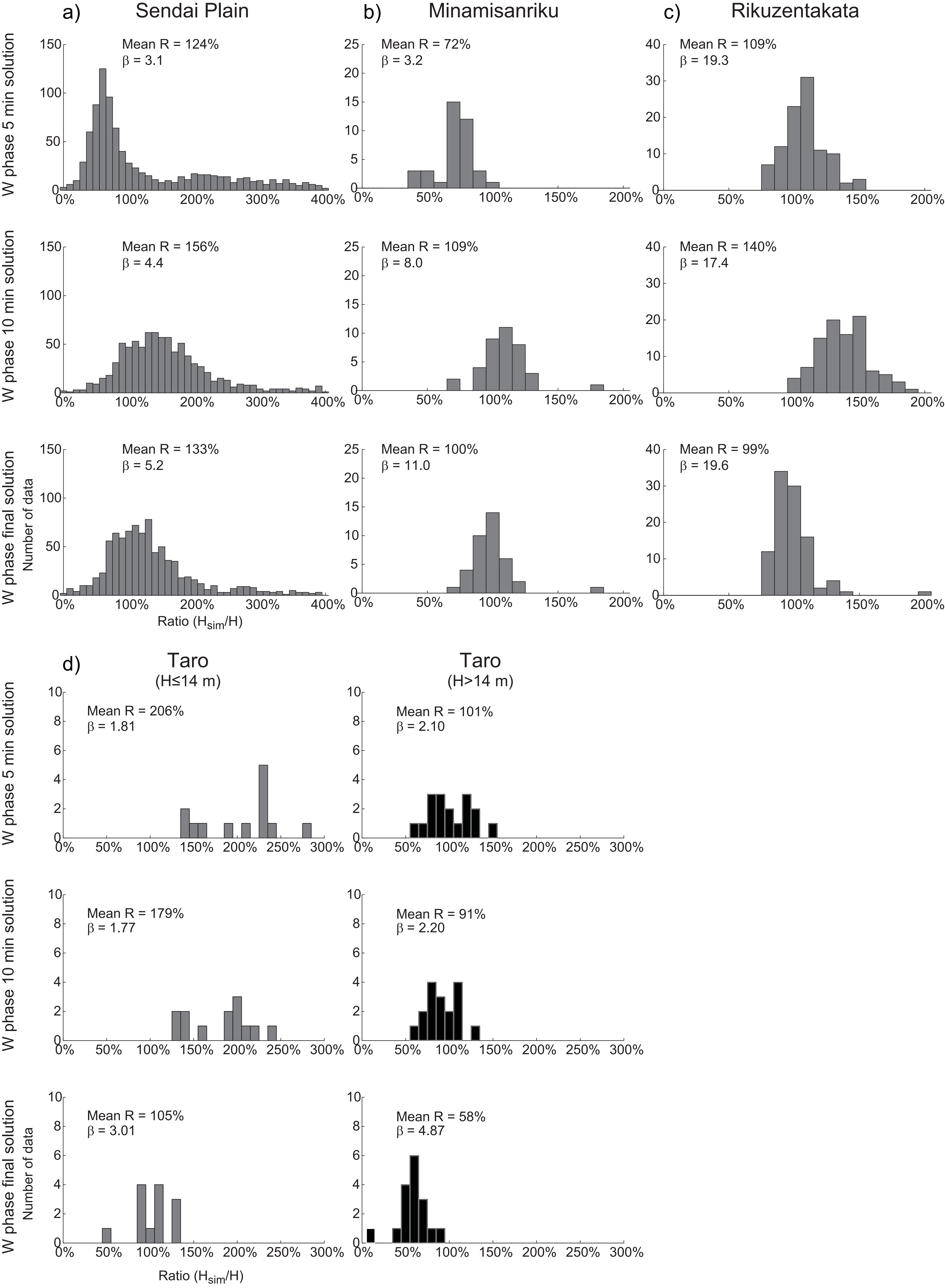

a) Sendai Plain
b) Minamisanriku
c) Rikuzentakata
W phase 5 min solution
W phase 10 min solution
W phase final solution
Number of data
Mean R = 124%
β = 3.1
Mean R = 72%
β = 3.2
Mean R = 109%
β = 19.3
Mean R = 156%
β = 4.4
Mean R = 109%
β = 8.0
Mean R = 140%
β = 17.4
Mean R = 133%
β = 5.2
Mean R = 100%
β = 11.0
Mean R = 99%
β = 19.6
Ratio (Hsim/H)
d) Taro (H≤14 m)
Taro (H>14 m)
Mean R = 206%
β = 1.81
Mean R = 101%
β = 2.10
Mean R = 179%
β = 1.77
Mean R = 91%
β = 2.20
Mean R = 105%
β = 3.01
Mean R = 58%
β = 4.87
Ratio (Hsim/H)

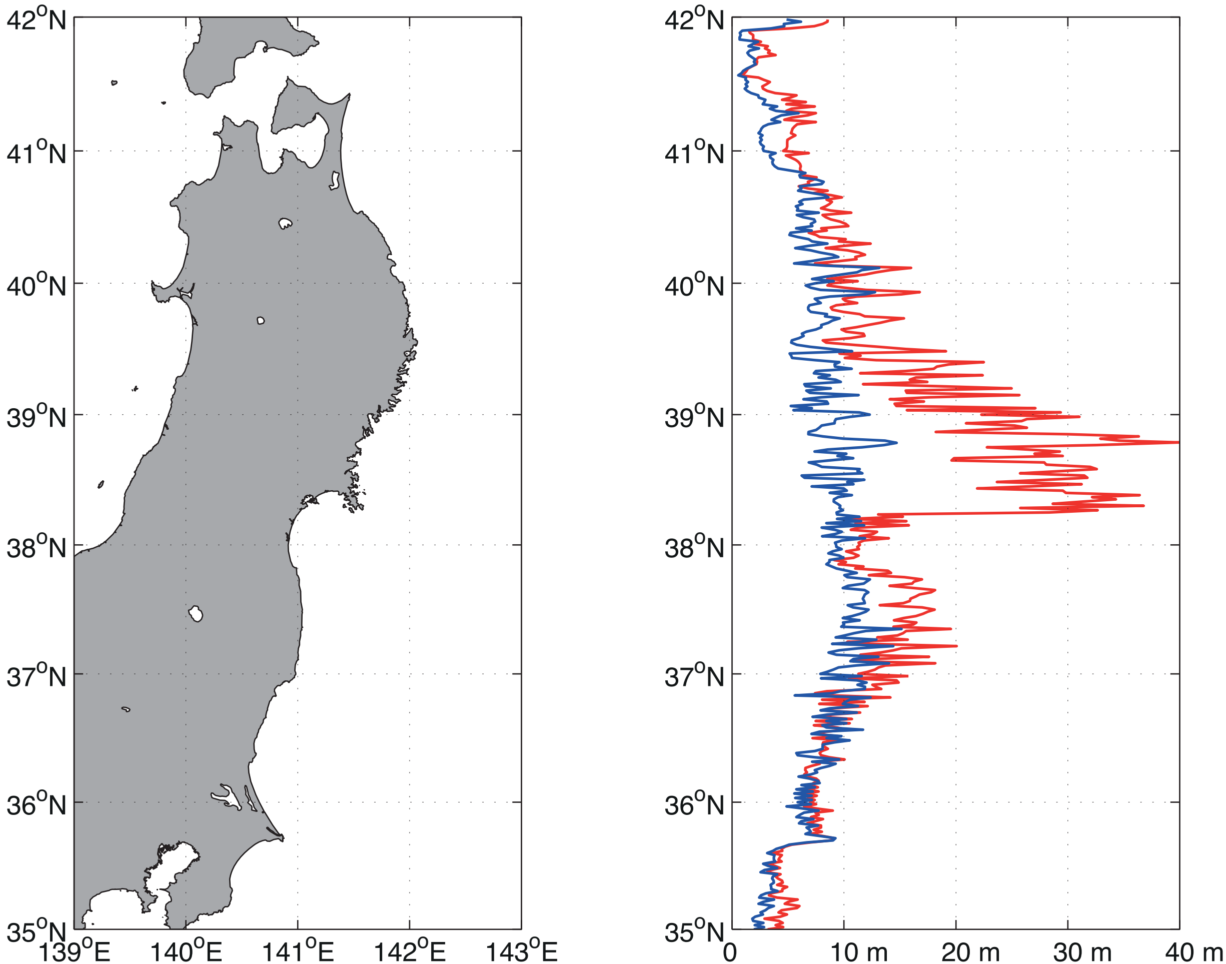

42°N
41°N
40°N
39°N
38°N
37°N
36°N
35°N
139°E
140°E
141°E
142°E
143°E
0
10 m
20 m
30 m
40 m